# Efficient variable time-stepping scheme for intense field-atom interactions

Charles Cerjan
*Lawrence Livermore National Laboratory, Livermore, California 94550*

Ronnie Kosloff
*The Fritz Haber Research Center for Molecular Dynamics, The Hebrew University, Jerusalem 91904, Israel*
(Received 1 June 1992)

The recently developed Residuum method [Tal-Ezer, Kosloff, and Cerjan, J. Comput. Phys. **100**, 179 (1992)], a Krylov subspace technique with variable time-step integration for the solution of the time-dependent Schrödinger equation, is applied to the frequently used soft Coulomb potential in an intense laser field. This one-dimensional potential has asymptotic Coulomb dependence with a "softened" singularity at the origin; thus it models more realistic phenomena. Two of the more important quantities usually calculated in this idealized system are the photoelectron and harmonic photon generation spectra. These quantities are shown to be sensitive to the choice of a numerical integration scheme: some spectral features are incorrectly calculated or missing altogether. Furthermore, the Residuum method allows much larger grid spacings for equivalent or higher accuracy in addition to the advantages of variable time stepping. Finally, it is demonstrated that enhanced high-order harmonic generation accompanies intense field stabilization and that preparation of the atom in an intermediate Rydberg state leads to stabilization at much lower laser intensity.

PACS number(s): 32.80.Fb, 32.80.Rm, 42.65.Ky

## I. INTRODUCTION

The experimental observation of nonperturbative effects in the photoejection spectrum and harmonic response of an atom coupled to an intense laser field has stimulated a well-developed theoretical effort to understand these phenomena. Some of the more interesting results obtained indicate the repeated absorption of photons by electrons which already lie in the ionization continuum—the so-called above-threshold ionization (ATI) effect—and the relatively efficient generation of higher-order harmonic photons generated by the atom. Since these observations cannot be understood by simple perturbative techniques, adequate theoretical explanation of these effects must necessarily include a more explicit, detailed treatment of the field-atom interaction.

The direct solution of the time-dependent Schrödinger equation by numerical methods is one such theoretical attempt to understand these experimental phenomena [1]. The major advantages that this approach possesses are those common to most numerical techniques: generality and highly detailed information. Some of the important experimental details can be readily incorporated into the numerical solution which might be difficult or impossible by other approaches. For example, if the temporal envelope of the applied laser field is not harmonic, which is likely experimental situation, then straightforward application of Floquet theory will not be possible. Also, complicated functional forms of the atomic potential can be used which are not simply Coulombic which thus renders basis-set choice and potential matrix evaluation difficult. Likewise, the numerical calculation of photoelectron spectra and harmonic generation can provide a large amount of detail that would be difficult for analytical methods to reproduce. Numerical techniques of course suffer from the endemic disadvantages of nonanalytical methods, such as the difficulty of demonstrating convergence and the associated problem of overwhelmingly large basis-function size or numerical grid size. Time-dependent methods are additionally constrained by the time scale of the temporal evolution of the problem; if the time steps are small and the duration of the event long then any such calculation might be intractable.

Strictly numerical attempts to solve the Schrödinger equation can be broadly classified as either time-independent or time-dependent methods. The former category typically expands the solution in an appropriate set of convenient basis functions, such as Sturmian functions [2], and then solves the associated energy characteristic value problem. The difficult part of these calculations is usually the evaluation of integrals over the chosen basis set. The second category typically uses a spatial grid and an approximation to the temporal evolution operator to generate a pointwise solution to the Hamiltonian operator. This class of methods does not require potential matrix evaluations, but it is usually limited by both the size of the spatial grid and by the time step controlling the accuracy of the evolving solution.

Grid methods have been used extensively to examine features of the intense field-atom interaction in one and several dimensions, especially simple differencing for the spatial derivatives and the Crank-Nicholson approximation to the exponential time evolution operator [1]. An alternative approach is to use a pseudospectral method—Fourier decomposition of the spatial derivatives—with some suitable choice of evolution operator [3]. Pseudospectral methods are capable of very high accuracy since they usually display exponential

 

rather than polynomial convergence rates. The Fourier decomposition also represents the typical asymptotic plane-wave expansion needed in potential scattering problems. The application of one such spectral technique to the intense field-atom interaction is described below. The next section (Sec. II) provides a brief introduction to the method; Sec. III presents the details of the one-dimensional Hamiltonian operator chosen and the numerical quantities used in the subsequent calculations; these calculations are discussed in Sec. IV and compared to previously published results. Section V contains a summary of the major points of this work.

## II. BACKGROUND

Given the complexity of a realistic multidimensional treatment of the intense field-atom interaction, some insight can be derived from the use of simplified one-dimensional formulations which retain some of the relevant physical features. The particular Hamiltonian operator which is the focus of the calculations presented in this work has the form

$$H(x,t)=\frac{\hbar^2}{2m}\left[p-\frac{e}{c}A(t)\right]^2+V(x) . \tag{2.1}$$

This operator describes the motion of an electron in the presence of the applied field $A(t)$, within the dipole approximation and with a stationary potential $V(x)$. The choice of atomic units for this operator removes several constants since $\hbar=e=m=1$. Following Javanainen, Eberly, and Su [4], the stationary potential is the "softened" Coulombic form

$$V(x)=-\frac{1}{(1+x^2)^{1/2}} , \tag{2.2}$$

which retains the asymptotic form of the Coulomb potential while reducing the singularity at the origin. The applied field will typically consist of two parts: an envelope function $A_0(t)$ multiplying a sinusoidal function of the laser frequency $\omega_l$.

The dynamics of the electron in this field can be monitored by two quantities which are experimental observables in the multidimensional case—the ejected-photoelectron spectra and the emitted-photon spectra. More specifically, if the evolving wave function is denoted by $\psi(x,t)$, then projection of the stationary (zero-field) bound states $\phi_n(x)$ from this wave function will provide a measure of the ionized electron components $\psi_c(x,t)$ at selected times. This projection yields

$$\psi_c(x,t)\approx\psi(x,t)-\sum_{n=0}^{N}(\psi(x,t),\phi_n(x))\phi_n(x) . \tag{2.3}$$

The amplitude of the spatial Fourier decomposition of this projection then approximately measures the probability of finding the ejected electron at different energies. This approximation is based on the assumption of negligible radiative relaxation to a bound state—all photoexcitation processes lead to dissociation.

The temporal dependence of the induced atomic dipole $\langle x(t)\rangle$ establishes the emitted-photon response, where

$$\langle x(t)\rangle\equiv\int_{-\infty}^{\infty}\psi^*(x,t)x\psi(x,t)dx . \tag{2.4}$$

The choice of this form neglects atom-atom correlations [5], but the overall simplicity of the one-dimensional treatment presented here does not warrant any more sophisticated calculation. In analogy to the ejected-electron spectra, the temporal Fourier transform of the induced dipole provides the energy dependence of the emitted photons.

Two different numerical schemes were used to investigate the time and space evolution of an initial wave packet centered in the stationary potential given by (2.2)—the well-known Crank-Nicholson propagator with spatial finite differencing [1] and the recently introduced Residuum method using a low-order Krylov subspace propagator with a pseudospectral spatial decomposition [6]. Krylov subspace techniques are known to have superior numerical efficiency, especially when used with the pseudospectral representation of the Laplacian operator [3]. These techniques supply an error estimate which can be used to control the time step chosen, thus offering the additional advantage of variable time stepping. In the interest of completeness, a brief description of the two different methods follows.

As mentioned above, there are two distinct numerical issues that must be addressed in the choice of a grid method for the time-dependent Schrödinger equation: the representation of the Laplacian operator on the grid and the choice of time-evolution operator using this spatial representation. Differencing methods follow from a local, low-order polynomial approximation to the differential operators occurring in the equation. Specializing to the Hamiltonian operator of (2.1), two differential operators appear, one for each power of the momentum. Following the notation of [4], these representations appear as

$$[H_0\psi(t)]_n=-\frac{1}{2(\Delta x)^2}[\psi_{n+1}(t)-2\psi_n(t)+\psi_{n-1}(t)]+V(x_n)\psi_n(t) , \tag{2.5}$$

and

$$[-p\cdot A\psi(t)]_n=\frac{iA(t)}{2\Delta x}[\psi_{n+1}(t)-\psi_{n-1}(t)] . \tag{2.6}$$

The $n$th spatial grid location is given by $x_n=n\Delta x$ for $n=-(N-1)/2$ to $(N-1)/2$ so that a subscript of a function denotes the value of the function at that grid point. A natural choice of boundary condition for the intense field problem is given by

$$\psi_{-(N-1)/2}(t)=\psi_{(N-1)/2}(t)=0 , \tag{2.7}$$

which was imposed upon all calculations. Higher-order polynomial approximations could be used, with the consequent tradeoff in computational effort. The use of a tridiagonal representation in (2.6) is simple and efficient.

Time propagation of the initial wave function can be accomplished rapidly and stably by a unitarized approximation to the true time-ordered exponential operator

$$U(t+\Delta t)=T\exp\left(-i\int_t^{t+\Delta t}H(s)ds\right) , \tag{2.8}$$

where $T$ denotes the time-ordering operator, by the rational fraction expression

$$U(t+\Delta t)\approx\left[1-\frac{i\Delta t}{2}H\left[t+\frac{\Delta t}{2}\right]\right]\times\left[1+\frac{i\Delta t}{2}H\left[t+\frac{\Delta t}{2}\right]\right]^{-1}. \tag{2.9}$$

Although this method is explicitly unitary, hence stable, its accuracy is only second order in the time expansion. It is well known that the Crank-Nicholson algorithm is dominated by dispersion error, which tends to produce an incorrect propagation speed of the associated Fourier components [7]. For multiple quantum reflections in the stationary well or for highly energetic ejected electrons, significant error could be introduced by this approach.

In contrast to the simple finite differencing plus Crank-Nicholson propagation (CN), a pseudospectral method with a low-order Krylov propagation (R) offers increased numerical efficiency. By analogy to (2.5), the spatial operation becomes

$$[H_0\psi(t)]_n=-\tfrac{1}{2}P^2\psi_n(t)+V(x_n)\psi_n(t)\ , \tag{2.10}$$

where

$$P^2\psi(x,t)=k^2\hat{\hat{\psi}}(k,t)\ , \tag{2.11}$$

where $\hat{f}(k,t)$ is the spatial Fourier transform of the function $f(x,t)$. That is, the operator is evaluated by first Fourier transforming the wave function at a given time $t$, multiplying by $k^2$, and then Fourier synthesizing to the original spatial grid. For functions localized on the grid, this operation is an identity; furthermore, the high computational efficiency of the fast Fourier transform algorithm can be directly applied to this representation. In many practical cases this approach supplies *exponential* convergence as compared with *polynomial* convergence for differencing schemes [8]. The remaining differential operator is calculated in the same manner,

$$[-p\cdot A\psi(t)]_n=iA(t)[P\psi(x,t)=ik\hat{\hat{\psi}}(k,t)]_n\ . \tag{2.12}$$

Note that it is straightforward to eliminate the dipole approximation in this representation; realistic spatial dependence for the vector potential $A(x,t)$ does not require exceptional treatment.

Time propagation can also be evaluated in a manner which has greater control of dispersion and phase errors. The approach adopted for this work entails the use of a low-order Kyrlov subspace calculation with error control supplied by the minimization of the so-called residual error in the subspace [6]. For a short time step, the full evolution operator (2.8) is approximated by the exponential operator which in turn can be expanded in terms of a low-order (order $m$) polynomial

$$e^{iH\Delta t}\approx\sum_{k=0}^{m}a_k(\Delta t)R_k(x)\ . \tag{2.13}$$

As in all Krylov subspace techniques, a subspace is generated for the operation of the evolution approximation by starting with an initial guess and iterating that guess in powers of the underlying operator. Thus the first basis vector is the initial vector $v_0=\psi(x,t)$ and subsequent vectors are generated by $v_j=H^jv_0$ for $j=1,\ldots,m$. The minimization of the error in this projected subspace with respect to a particular operator generates the matrix equation

$$A\delta=b\ . \tag{2.14}$$

The $(i,j)$th component of the matrix $A$ is given by the inner product of the iterated vectors, $A_{i,j}=(H^iv,H^jv)$, and the $i$th component of the vector $b$ is $b_i=-(H^iv,v)$. The solution vector $\delta$ provides the coefficients of the residual error polynomial; the roots of the polynomial are the interpolation points of the original polynomial approximation to the exponential evolution operator. Time-step control is achieved by monitoring the $l_2$ norm of the residual vector; a value greater than a specified error tolerance forces a time-step reduction and an iteration of the procedure.

## III. INTENSE FIELD-ATOM APPLICATIONS

The methods described above were used in a variety of contexts emphasizing different choices of laser frequency, pulse duration, and temporal envelope. Since the initial-time wave function is taken to be the ground state of the "softened" Coulomb and the field-free bound states are needed for the projection in (2.3), a suitable representation of these functions on the grid is required. For the differencing method, the grid choice of Javaninen, Eberly, and Su [4] is reasonable: the total number of grid points was 32 001 with a grid spacing of $\Delta x=0.0707$ bohr. The ground state and first 30 bound states were evaluated by inverting the difference matrix representation of the Hamiltonian operator. These values reproduce previously reported values [4]. Identical accuracy (within $10^{-5}$) for the pseudospectral representation of the *energies* of the same bound states was obtained by using a grid of 4096 points with a grid spacing of $\Delta x=0.50$ bohr. These states were evaluated by propagating the Hamiltonian operator in imaginary time after successively filtering the previously determined lower bound states [3].

Since all the calculations were performed in the $p\cdot A$ gauge, the relation between the electric field $E$ and vector potential must be used:

$$A(t)=-\int_0^t E(s)\sin(\omega_l s)ds\ . \tag{3.1}$$

The various temporal electric fields which were examined were the square pulse

$$E(t)=\begin{cases}E_0 & \text{if } 0\le t\le T_c\\ 0 & \text{otherwise}\ ,\end{cases} \tag{3.2}$$

a full smooth pulse

$$E(t)=\begin{cases}e_0\sin^2(\pi t/T_c) & \text{if } 0\le t\le T_c\\ 0 & \text{otherwise}\ ,\end{cases} \tag{3.3}$$

and a smooth turnon pulse

$$E(t)=\begin{cases} E_0 \sin^2(\pi t/2T_c) & \text{if } 0 \le t \le T_c \\ E_0 & \text{if } t > T_c \ . \end{cases} \tag{3.4}$$

The parameter $T_c$ determines the envelope of the pulse and is chosen to be a multiple of the optical cycle time.

The choice of temporal envelope for the applied laser pulse can influence the computational results dramatically. An obvious qualitative difference is the application of the laser for only a select number of field cycles. The asymptotic time analysis then becomes well defined on the grid. Conversely, a smooth turnon with nonterminating field, for example, Eq. (3.4) above, renders the wave packet analysis difficult. One reasonable procedure is to analyze the evolved wave function at the end of a field period. This choice is not completely satisfactory since relaxation effects might not be properly accounted. These effects have been addressed previously [4] and need not be elaborated here. It should be emphasized that the choice of the initial temporal shape was not found to be critically important provided that the field maximum was achieved after 5–10 field cycles in a relatively smooth fashion.

The first application follows that of Eberly, Su, and Javanainen [9], who applied the finite differencing scheme with a Crank-Nicholson time propagation to a square pulse field with an amplitude $E_0=0.04$ a.u., a frequency $\omega_l=0.07$ a.u., and a pulse duration $T_c=16.25$ field cycles. The time step $\Delta t=0.08$ a.u., which corresponds to approximately 1122 time steps for each optical cycle. Since the ground-state energy of the potential is $-0.670$ a.u., this frequency corresponds to ten-photon ionization. The generation of high-order harmonic frequencies is prominently displayed in Fig. 1, especially odd harmonics of the applied field. The intensities are all scaled to the largest value and their logarithms plotted on the vertical axis.

The Residuum method was applied to this case also and the results of this calculation are plotted in Fig. 2. The grid parameters were selected as noted above with variable time stepping. A fifth-order polynomial approximation was chosen for the short-time propagation step with a specified error tolerance of $10^{-7}$. The average number of time steps for each optical cycle was approximately 2278, which is an average time step of 0.039 a.u. Almost all of the prominent features of the spectrum agree between the two calculations, which implies that a lower-order scheme might be suitable for this case.

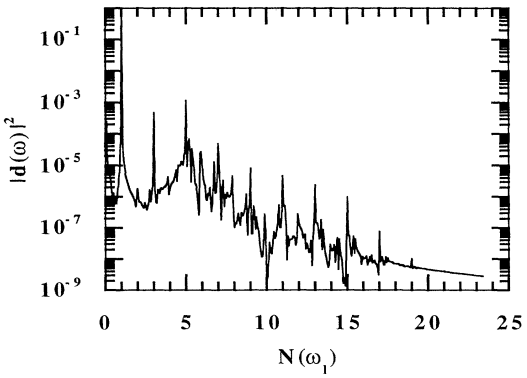


FIG. 1. The absolute magnitude of the temporal Fourier transform of the dipole moment function plotted against the energy in units of the field frequency for Crank-Nicholson propagation with $E_0=0.04$ a.u. and $\omega_l=0.07$ a.u. A square pulse was applied for a total of 16.0 field cycles.

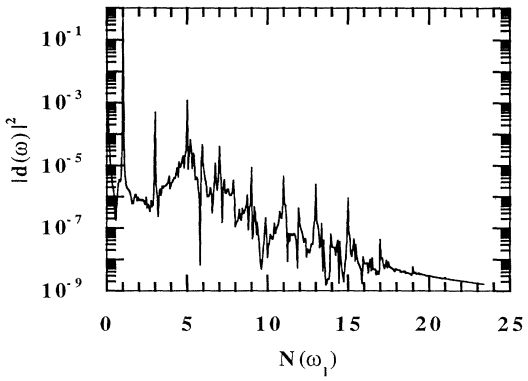


FIG. 2. The same as Fig. 1 for Residuum propagation.

The second application represents two-photon ionization from the static potential, namely, $\omega_l=0.52$ a.u. The field amplitude $E_0$ was chosen to be 0.05 a.u. with a full smooth pulse of duration $T_c=96$ field cycles. The predicted harmonic generation and ATI spectra are given in Figs. 3(a) and 3(b), respectively, for the simple

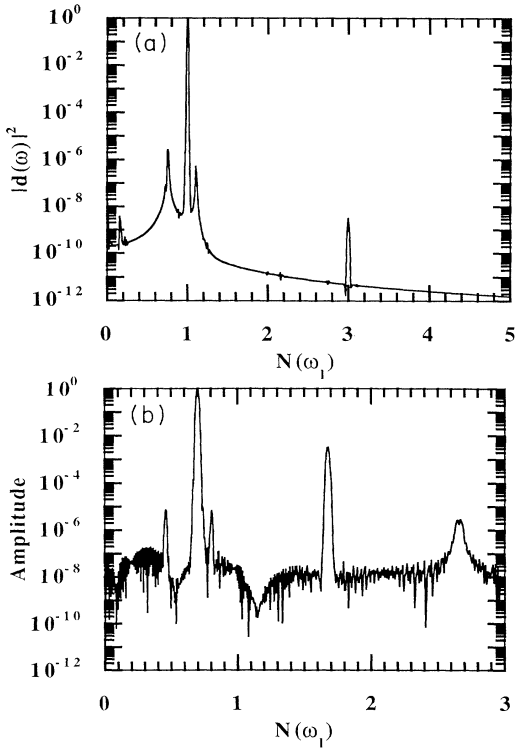


FIG. 3. (a) Harmonic generation spectra for Crank-Nicholson propagation with $E_0=0.05$ a.u., $\omega_l=0.52$ a.u., and a 96-cycle smooth pulse turnon. The energy is plotted in units of the applied field frequency. (b) ATI spectra for the conditions of (a).

differencing algorithm. The corresponding spectra from the Residuum method are plotted in Figs. 4(a) and 4(b). The intensities in all cases were scaled to the largest value for comparison; the vertical axis is again logarithmic. An examination of the figures reveals a substantive difference between the two methods.

The ATI spectra bear only a qualitative resemblance to one another; the Residuum method predicting that very little of the initial wave packet is energetically excited above the ionization threshold, but with an extensive amount of structure in the energy spectrum. The largest spectral peak is centered about the excess ionization energy of 0.370 a.u. ($0.70\omega$) from resonant two-photon absorption from the ground state. The other prominent features in the ATI spectrum are likely due to a few dominant absorption mechanisms: the peak at $0.46\omega$ is probably one-photon absorption from the first excited state; the peaks at $1.68\omega$ and $2.65\omega$ are three- and four-photon ionization from the ground state. It should be noted that within the numerical accuracy of the calculation, these multiple photon peaks could also have contributions from excitations from the second excited state but these are expected to be weak transitions, at least lower field intensities. Finally, the Residuum plot displays a series of near-threshold maxima separated by approximately $0.05\omega$. These features cannot be resolved in the finite difference calculation. This separation does not correspond to the ponderomotive shift, which is $0.0044\omega$ for these conditions.

Similarly, the harmonic spectra reveal a great deal of structure in the Residuum calculation which is absent in the differencing calculation. Several subharmonic contributions to the dominant integral photon emission processes can be discerned. Since the total probability of ionization is quite small under these conditions, multiple transitions among the many field-free bound states are expected. The qualitative physical process is thus predicted to be quite different since many more localized (bound) interference effects are exhibited by these results. The subharmonic contributions from the initial turnon of the pulse is probably more influential in this case also.

The third and final application is suggested by Su and

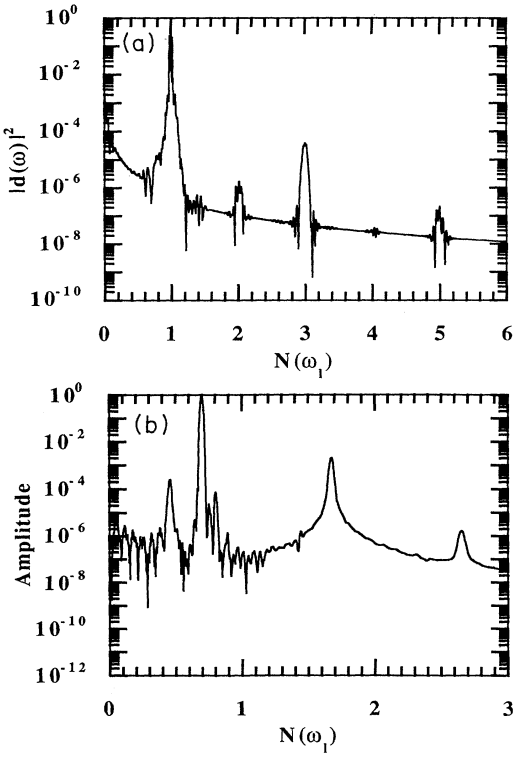


FIG. 4. (a) Same plot as Fig. 3(a) for Residuum propagation. (b) Same plot as Fig. 3(b) for Residuum propagation.

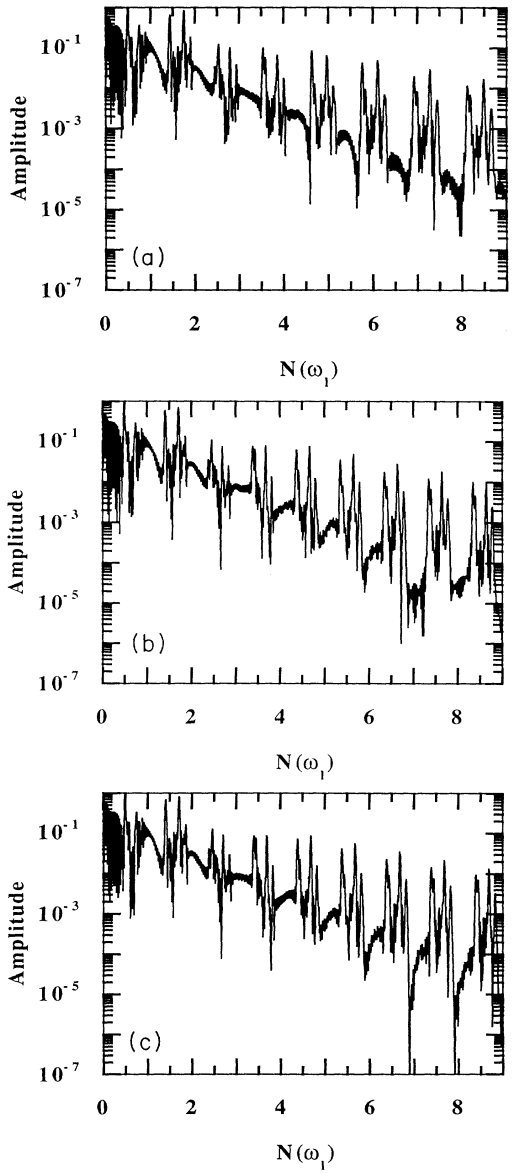


FIG. 5. (a) ATI spectra plotted against the energy in units of the applied field frequency for Crank-Nicholson propagation for a smooth pulse turnon of 5.25 cycles, $E_0=2.0$ a.u., $\Delta t=0.08$ a.u., and $\omega_l=0.52$ a.u. The simulation was stopped at 16.25 cycles. (b) Same plot as (a) for variable-time-step Residuum propagation. (c) Same plot as (a) for Crank-Nicholson propagation with $\Delta t=0.01$ a.u.

Eberly in their investigation of intense-field stabilization [10]. Relative suppression of ionization was observed as the field was increased; that is, the probability of ionization at a field amplitude $E_0=1.0$ a.u. is about 0.80, whereas that at $E_0=5.0$ a.u. is about 0.55 at the same time (400 a.u.). This trend can be qualitatively explained by reflection from the time-dependent potential term $p\cdot A(t)$, which, at sufficiently large amplitude, can return a significant fraction of the ionized wave function to the center of the stationary potential where it can again absorb and emit photons. Indeed, plots of the time-dependent projection of the wave function onto the field-free ground state reveal the repopulation of this state as the field intensity increases.

Figure 5(a) contains a logarithmic plot of the higher-order harmonic spectra as a function of energy in units of the applied field frequency predicted by the differencing method for a field amplitude of 2.0 a.u.; the corresponding plot for the Residuum method is shown in Fig. 5(b). The parameter $T_c=5.25$ field cycles for a smooth turnon of the field, which had a duration of 32.25 cycles. The time step for differencing was initially set to 0.08 a.u., while the average time step for the Residuum method was 0.02 a.u. The time step was reduced to 0.01 a.u. for this case, $E_0=2.0$ a.u., using the differencing method, and these results are shown in Fig. 5(c).

Although the qualitative structure of the spectra match for all three cases, closer inspection reveals that the 0.08-a.u. time step has a systematic shift to higher energy. For example, at 6 photon units the 0.08-a.u. time-step calculation places the ATI peak at 6 units rather than somewhat lower. The smaller time-step calculation corrects this inaccuracy in the lower-energy range, but a similar error eventually reappears between 20 and 25 photon units. Figures 6(a) and 6(b) corroborate this claim. These are the analogous plots to the previous figures. The 0.01-a.u. time step is in obvious disagreement with the other calculation even with a smaller time step than the average time step for the variable stepping method.

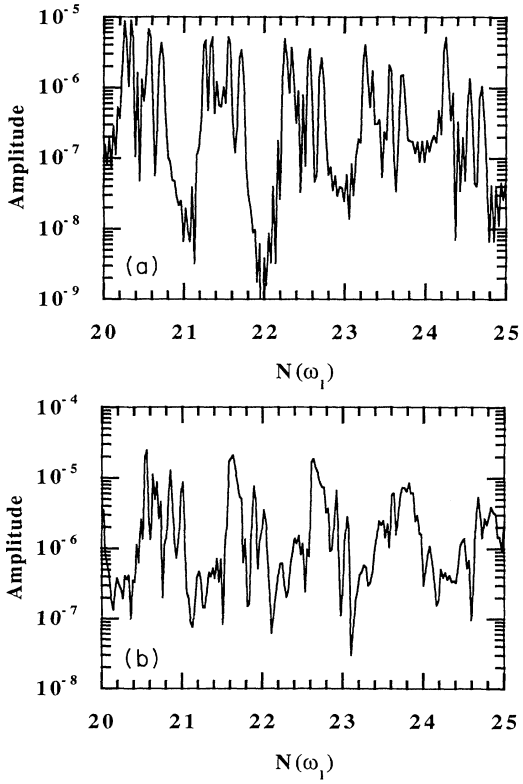


FIG. 6. (a) ATI spectra for the conditions of Fig. 5(b) with the higher energy range displayed. (b) Same as Fig. 5(c) with the higher energy range displayed.

## IV. COMPARATIVE ANALYSIS

The above calculations display obvious discrepancies which can be traced to at least two major differences. First, the choice of grid for the simple differencing scheme is adequate for the determination of the energies of a large number of bound states but it is inadequate for the determination of properties such as the time-dependent dipole moment or, correspondingly, the time-dependent momentum expectation value. Second, the relative phase and dispersion error introduced by the Crank-Nicholson expression can seriously compromise quantum interference effects within the stationary potential well or can spread the evolving wave packet too quickly over the grid. In contrast to this behavior, the pseudospectral representation appears to maintain higher accuracy for the calculation of wave-function properties while the variable time-step propagation more accurately follows the changes in phase and dispersion as the evolution progresses.

In order to investigate the numerical representations more fully, the time dependence of the problem was removed and a comparison to the Chebyshev propagation technique was attempted [3]. The choice of a spatially compact initial state which is localized on either grid will provide a direct comparison of the time propagation schemes. The specific form of this initial state was chosen to be

$$\psi(x,0)=(1+x+x^2+x^3)e^{-x^2/\sigma^2}\ , \tag{4.1}$$

with $\sigma=4.0$. The energy of this state is $-0.2952$ hartree with an overlap of 0.601 with the ground state of the potential. The polynomial factor ensures that there will be some overlap with the remaining bound states so that this wave function represents an approximation to a wave function evolved in the presence of a field with multiphoton excitations present.

The grids described above were used for the spatial representation: $\Delta x=0.0707$ a.u. and $N=32\,001$ for the differencing grid and $\Delta x=0.50$ a.u. and $N=4096$ for the pseudospectral grid. Three different time evolution methods were used: Chebyshev, Residuum, and Crank-Nicholson. The Chebyshev method is capable of machine accuracy and thus can be used as a standard against which to compare the others. The initial state was then evolved with a time step of 0.08 a.u. and the dipole moment calculated as a function of time. The difference between the Chebyshev and Crank-Nicholson

calculations is plotted in Fig. 7(a). The corresponding difference between the Chebyshev and Residuum methods was the requested tolerance of $1.0\times10^{-7}$ for the entire time sampled; hence it is not plotted. It is clear that there are errors in phase and amplitude generated by the Crank-Nicholson algorithm since the Crank-Nicholson prediction oscillates in phase about the correct value even at the earliest times. The envelope of the difference is linearly increasing with time, indicating a growing error in amplitude as the wave function evolves. The growth in the amplitude difference can be controlled by decreasing the time step for the Crank-Nicholson propagator as demonstrated in Fig. 7(b). In this figure, the time step has been reduced to 0.04 a.u. and then compared to the Chebyshev value at the larger time step of 0.08 a.u. The frequency of the oscillations about the correct value is not affected by the decreased time step though, indicating that phase errors will be quite difficult to control in the Crank-Nicholson scheme.

Returning to one of the applications above ($E_0=0.05$ a.u. with $\omega_l=0.52$ a.u. and a smooth turnon of 96 cycles), it is perhaps worthwhile to examine the differences between the temporal variation of the two calculations—variable time stepping compared to the fixed-step results. The difference between the $\Delta t=0.08$ and variable time step time-dependent dipole moments is plotted in Fig. 8(a) as a function of time. Both phase and amplitude differ with the fixed-time-step evaluation alternately larger and smaller than the variable time step. The difference is especially pronounced during the rise and fall times of the field envelope but less so at the maximum, where the envelope is relatively slowly varying. The differences in the calculated dipoles closely follows the applied field frequency, as demonstrated in Fig. 8(b), where the difference of the dipole moments is plotted as a function of time in units of the field cycle for 20 cycles between 20 and 40 cycles. The overall phasing difference accounts for the discrepancy seen between Figs. 3 and 4. Since the wave function remains bound throughout the pulse (less than 0.01 is ionized), multiple interference effects within the potential might contribute to the harmonic spectra leading to even-order peaks.

The importance of the accurate evaluation of the momentum operator and the phase change at the turning points of the static potential can be qualitatively addressed by examining the full time-dependent solution to the Schrödinger equation in (2.1). Designate some known part of the Hamiltonian operator as $H_0$, so that the transformation

$$\psi(x,t)=\exp(-iH_0t)\phi(x,t) \tag{4.2}$$

reduces the original equation to

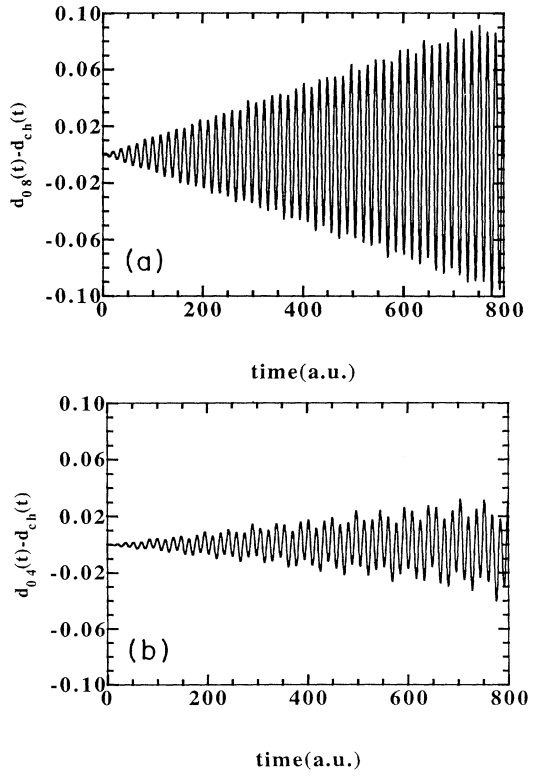


FIG. 7. (a) The difference between the dipole moments calculated for the zero-field case using Crank-Nicholson propagation [$d_{08}(t)$] and Chebyshev propagation [$d_{ch}(t)$] with a fixed time step of $\Delta t=0.08$ a.u. as a function of time. (b) Same as (a) with a fixed time step of 0.04 a.u. for the Crank-Nicholson propagation.

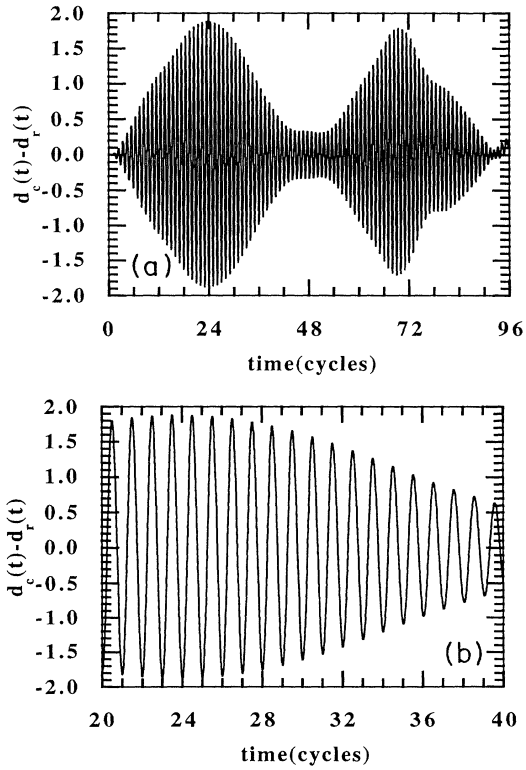


FIG. 8. (a) The difference between the dipole moments calculated for the smooth turnon 96-field cycle calculation of Fig. 3(a) between the Crank-Nicholson [$d_c(t)$] and the Residuum result as a function of time in units of the field cycle time. (b) An expanded view of (a) for the time between 20 and 40 field cycles.

$$-i\frac{\partial\phi(x,t)}{\partial t}=e^{iH_0t}W(x,t)e^{-iH_0t}\phi(x,t)\ , \tag{4.3}$$

where $W(x,t)$ is the remaining part of the operator. Choosing $H_0$ to be the static part of the original operator, which is a better representation in the weak-field limit, leads to

$$-i\frac{\partial\phi(x,t)}{\partial t}=-\frac{A(t)}{c}(e^{iH_0t}pe^{-iH_0t})\phi(x,t)\ . \tag{4.4}$$

Using the well-known commutator expansion for operators $A$ and $B$ [11],

$$e^{A}Be^{-A}=B+[A,B]+[A,[A,B]]/2!+\cdots\ , \tag{4.5}$$

the importance of the momentum operator and potential derivatives is immediate,

$$(e^{iH_0t}pe^{-iH_0t})=p+it[H_0,p]+(it)^2[H_0,[H_0,p]]/2!+\cdots\ . \tag{4.6}$$

For a small time interval $\Delta t$, the evolving solution has the form

$$\psi(x,t+\Delta t)\approx e^{-iH_0\Delta t}e^{if_1(\Delta t)[p-i(\partial V/\partial x)]}\phi(x,t)\ , \tag{4.7}$$

where $f_1(\Delta t)=\int_t^{t+\Delta t}A(s)ds$.

This expression displays the Kramers-Henneberger time translation explicitly and the role of the static potential derivatives (or equivalently the momentum commutator evaluation) in determining the wave-function phase. The derivatives are largest at the classical turning points of the motion, which is an equivalent way of stating that interference effects are most pronounced at these turning points. In the limit that the applied field dominates the static potential, a better representation would be choosing the Volkov states as the homogeneous solution, or in the time-dependent formulation above,

$$H_0(x,t)=\frac{p^2}{2}-\frac{A(t)}{c}p \tag{4.8}$$

and

$$W(x,t)=V(x)\ . \tag{4.9}$$

Using the commutator expansion to obtain a first-order solution leads to

$$\psi(x,t+\Delta t)\approx e^{iV(x)\Delta t}\exp\left[\frac{i\Delta tp^2}{2}-\frac{f_1(\Delta t)}{c}p\right]\phi(x,t)\ . \tag{4.10}$$

Again, the time translation appears naturally and the potential does not influence the harmonic spectrum if its derivatives are ignored. Thus the harmonic spectra should not be as sensitive to interference effects confined to the potential well; indeed, two intense-field cases, $E_0=2.0$ and 5.0 a.u., produced nearly identical harmonic generation using either numerical method. On the other hand, when interference effects are important, physically relevant details can be overwhelmed by errors in the phase and dispersion. These quantities should then be strictly controlled throughout the temporal evolution.

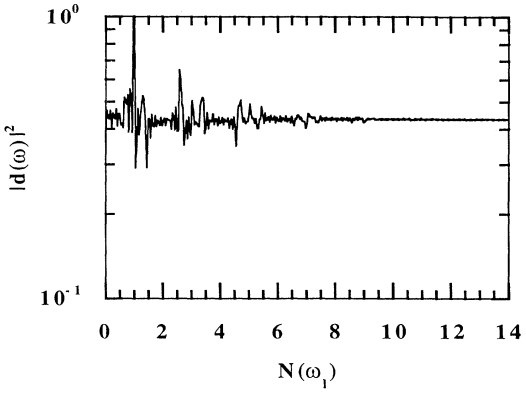


FIG. 9. Harmonic spectra generated by the conditions of Fig. 5 for a field amplitude of $E_0=1.0$ a.u. as a function of energy in units of the applied field.

Finally, the advantages of the variable time-stepping procedure are paramount when examining frequency-dependent effects, especially in the approach to the static field limit. As an example of this advantage, the onset of the so-called stabilization effect as a function of applied field frequency can be readily investigated. When stabilization occurs, the ionization probability as a function of intensity no longer increases. Furthermore, since the particle remains more localized near the center of the potential well, there is enhanced absorption and emission. The harmonic spectra, calculated in the acceleration gauge [12], expected for a field strength of 1.0 a.u. is plotted in Fig. 9; this field strength is immediately below the stabilization limit for this case. Once the field is increased to 2.0 a.u., stabilization occurs and the generated harmonic spectrum contains a great deal of structure, as displayed in Fig. 10. The question arises whether it might be possible to obtain stabilization, and consequent high-order harmonic generation, at lower intensities.

It might be expected that preparing the system so that some higher bound state is initially populated could lower the threshold for stabilization since a less intense field should have more effect on a particle in an intermediate or high Rydberg state [13]. A series of calculations was performed assuming that the $n=8$ state ($E_8=-0.0217$ hartree) was initially populated. The evo-

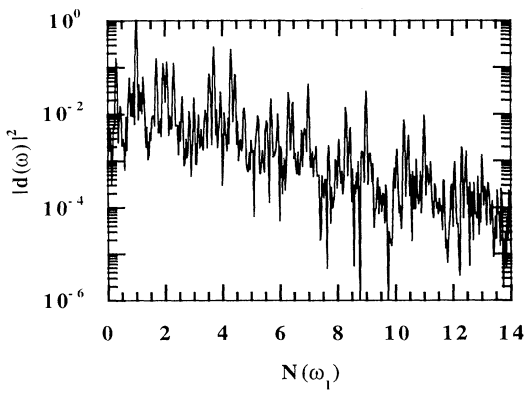


FIG. 10. Same as Fig. 9 for $E_0=2.0$ a.u.

TABLE I. Ionization probability after ten field cycles as a function of intensity in W/cm$^2$ for an initial state prepared in the $n=8$ stationary state for applied frequencies of 0.015 and 0.060 a.u. (numbers in brackets refer to powers of ten).

| $I_{0.015}$ | Fraction ionized | $I_{0.060}$ | Fraction ionized |
|---|---|---|---|
| 1.0[10] | 0.06 | 1.0[12] | 0.22 |
| 1.0(12) | 0.85 | 1.0(13) | 0.50 |
| 1.0(13) | 0.68 | 1.0(14) | 0.70 |
| 5.0(13) | 0.36 | 2.5(14) | 0.69 |
| 1.0(14) | 0.37 | 5.0(14) | 0.54 |
| | | 1.0(15) | 0.54 |

lution of the wave packet was followed for ten field cycles using two different applied field frequencies. The results of these calculations are given in Table I. There is clearly a strong frequency dependence to the onset of stabilization, with the threshold occurring about $5.0\times10^{13}$ W/cm$^2$ for $\omega_l=0.015$ a.u. and at $5.0\times10^{14}$ W/cm$^2$ for $\omega_l=0.060$ a.u. These preliminary results suggest that a "two-color" experiment could effectively lower the stabilization threshold and produce high-order harmonic generation at relatively low field intensities.

## V. SUMMARY

The investigation of intense-field interactions with atomic systems places stringent demands on any numerical solution. The method of choice must be capable of accurately following the development of the interaction from the weak-field case when the interaction is initiated to peak intensity conditions. Variable time stepping is clearly a major advantage in this regard, especially if many field cycles are required to simulate the true temporal laser-pulse shape. Furthermore, it is essential that the grid representation selected provide an accurate evaluation of the properties of the evolving wave function. Since these numerical studies are then analyzed for insight into the physical mechanism of intense-field stabilization, reliable predictions of level populations must be obtained, and these values are sensitive to properties calculated with the wave function. The applications discussed above demonstrate that the loss of phase information can seriously compromise the predicted harmonic photon spectra since various orders of emitted photons will be sensitive to the details of the initial weak-field evolution. Likewise, uncontrolled dispersion error leads to erroneously shifted ejected-electron spectra. Semilocal methods such as finite differencing will fail for long-time evolution. They compromise both the position-momentum commutation relation and the time-energy uncertainty relation. The consequence of these errors is that the error in phase-sensitive quantities will always surface for long times in the finite difference schemes. The application of these methods then relies on extracting useful physical information before these inherent errors overwhelm the calculation.

The choice of a pseudospectral grid representation with variable time-step control offers a powerful alternative to other numerical grid methods. In the above applications, the grid spacing was about seven times larger for the pseudospectral method than for the differencing grid with superior accuracy. This reduction in the number of grid points resulted in a factor of 35 increase in computational speed when both methods were used for a fixed number of time steps. With the additional advantage of variable time stepping, another twofold increase in efficiency was often achieved.

The great flexibility afforded by numerical grid methods accounts for their widespread use in the study of intense field-atom interactions. The applications above emphasize the need for an accurate and computationally tractable method of solution. These requirements can be met by the Residuum method. Extensions of these one-dimensional results are required to provide more detailed comparison with experiments; the relatively small grids required in this Coulomb-like potential indicate that accurate higher-dimensional calculations will be possible.

## ACKNOWLEDGMENTS

Work at the Lawrence Livermore National Laboratory is performed under the auspices of the U.S. Department of Energy, administered by the University of California under Contract No. W-7405-Eng-48. Work at the Fritz Haber Institute is supported by the Minerva Gesellschaft and the U.S.-Israel Binational Science Foundation.

[1] K. C. Kulander, K. J. Schafer, and J. L. Krause, in *Atoms in Intense Radiation Fields*, edited by M. Gavrila, Advances in Atomic, Molecular, and Optical Physics, Suppl. 1 (Academic, New York, 1992), p. 247.

[2] R. V. Weaver, J. T. Muckerman, and T. Uzer, in *Time Dependent Quantum Molecular Dynamics*, edited by J. Broeckhove (Plenum, New York, in press).

[3] C. Leforestier, R. Bisseling, C. Cerjan, M. Feit, R. Friesner, A. Guldberg, A. Hammerich, G. Jolicard, W. Karrlein, H. D. Meyer, N. Lipkin, O. Roncero, and R. Kosloff, J. Comput. Phys. **94**, 59 (1991); C. Cerjan and R. Kosloff, J. Phys. B **20**, 4441 (1987).

[4] J. Javanainen, J. Eberly, and Q. Su, Phys. Rev. A **38**, 3430 (1988); Q. Su and J. H. Eerly, *ibid.* **44**, 5997 (1991).

[5] B. Sundaram and P. W. Milonni, Phys. Rev. A **41**, 6571 (1990).

[6] H. Tal-Ezer, R. Kosloff, and C. Cerjan, J. Comput. Phys. **100**, 179 (1992).

[7] C. A. J. Fletcher, *Computational Techniques for Fluid Dynamics* (Springer-Verlag, New York, 1987), Vol. I, Chap. 9.

[8] E. Tadmor, SIAM J. Numer. Anal. **23**, 1 (1986); D. Gottlieb and S. A. Orszag, *Numerical Analysis of Spectral Methods: Theory and Applications* (SIAM, Philadelphia, 1977).

[9] J. H. Eberly, Q. Su, and J. Javanainen, Phys. Rev. Lett. **62**, 881 (1989).

[10] Q. Su and J. H. Eberly, J. Opt. Soc. Am. B **7**, 564 (1990).

[11] R. M. Wilcox, J. Math. Phys. **8**, 962 (1967).

[12] K. Burnett, V. C. Reed, J. Cooper, and P. L. Knight, Phys. Rev. A **45**, 3347 (1992).

[13] K. Burnett, P. L. Knight, B. R. M. Piraux, and V. C. Reed, Phys. Rev. Lett. **66**, 301 (1991).